



ACOUSTICS 2012

Use of short range outdoor sound propagation and acoustic-to-seismic seismic coupling to deduce soil state

H.-C. Shin^a, S. Taherzadeh^a, K. Attenborough^a and W.R. Whalley^b

^aThe Open University, DDEM, Maths, Computing and Technology, Walton Hall, MK7 6AA
Milton Keynes, UK

^bRothamsted Research, West Common, AL5 2JQ Harpenden, UK
h.c.shin@open.ac.uk

In agriculture, the soil structure, moisture content and strength have profound effects on plant growth. When soils are regarded as porous media, sub-surface wave propagation can be indicative of the soil status. Such propagation can be initiated by sources of airborne sound through acoustic-to-seismic coupling. Measurements of the ratio of near-surface sound pressure to acoustically induced solid particle motion can be exploited to estimate the acoustic and elastic properties of soils. Traditional methods of monitoring seismic signals by use of buried geophones are invasive and may affect the soil samples of interest. This paper describes a non-invasive acoustic-seismic technique. A loudspeaker was used to generate airborne sound, and the reflected sound and the subsequent vibration of the soil surface were recorded by microphones and a laser Doppler vibrometer respectively. These data were used to estimate acoustic and elastic soil parameters through an optimisation process minimising the differences between the data and model predictions based on incorporation of a modified Biot theory in a wave propagation model. Example results of laboratory and field measurements are reported.

1 Introduction

Acoustic-to-seismic (A-S) coupling is a phenomenon whereby seismic wave propagation inside soils is initiated by an airborne acoustic sound. The top layers of soils are usually more porous and less dense than deep layers due to weathering and plant growth and are therefore more likely to support the seismic motion induced by acoustic means [1]. A-S coupling has been used to detect buried landmines containing a resonant air cavity by mapping the anomalous acoustically-induced soil particle motion immediately above the landmine using a laser Doppler vibrometer (LDV) [2].

Outdoor sound propagation over a ground has been extensively investigated [3, 4]. Typically the ground has been acoustically characterised by a surface impedance which can be deduced from either the excess attenuation [5] or level difference [6] with the aid of sound propagation models. The deduced surface impedance spectra are then analysed further to estimate several physical parameters such as porosity.

Among the models of wave propagation, the reflected field of an incoming spherical wave from a monopole point source over a flat reflecting surface is well known through the Sommerfeld integral in the context of both electromagnetism and acoustics [7]. For a long-range sound propagation, the integral was simplified by identifying the poles of the plane-wave reflection coefficient [8]. The ground was idealised as a rigid-frame porous material. For a typical outdoor ground with a low pore-borne wave speed, the ground soil has been treated as locally-reacting. Subsequent work has allowed the ground to be extended or bulk reacting [9].

Although the assumption of a rigid frame is satisfactory for predicting sound propagation above the ground, it is not adequate to explain the response of a buried geophone to sound waves incident on the ground surface [10]. For this type of A-S coupling, it may be necessary to consider the ground soil to be poro-elastic rather than poro-rigid. Maurice A. Biot identified three types of elastic waves propagating in a fluid-saturated porous elastic solid: type-I and -II compressional waves and a shear wave [11]. When Biot's poroelasticity theory is combined with wave propagation model in layered media, it has been shown that the wave propagation can be modelled above and under non-rigid ground from a monopole acoustic source [12]. This modelling is used for the current work to deduce the physical parameters of soils. A-S coupling has been measured on unconsolidated sand in a laboratory [13] and also on a flat open field [1] using an LDV and a microphone. A compression driver with an extension tube was used to generate airborne sound, and the reflected sound and the subsequent vibration of the soil surface were recorded by microphones and an LDV respectively.

These data, all non-invasively obtained, were used to estimate acoustic and elastic/seismic soil parameters using an optimisation process minimising the differences between the data and model predictions.

2 Methods

2.1 Biot-Stoll poroelasticity model

For Biot poroelasticity theory, we need a certain number of physical parameters to describe the wave propagation within an air-saturated unbounded homogenous and isotropic poroelastic material. First set of required parameters define the properties of interstitial air within porous frame. They are density (ρ_f), dynamic viscosity (η), atmospheric pressure (P), specific heat ratio (γ), and Prandtl number of air (N_{pr}). These are well documented and hence can be treated as known constants. When these are combined with a model for pore shape and structure, one can define the bulk modulus of the interstitial air (K_f):

$$K_f = (\gamma P) / \left[\gamma - (\gamma - 1)H(\lambda \sqrt{N_{pr}}) \right] \quad (1)$$

Here, $H(\cdot)$ is a correction factor to account for the deviation of the interstitial air density from that of free air, and has been calculated for many ideal pore shapes [4]. The viscosity correction factor ($F(\cdot)$) for a two-dimensional pore shape was introduced in Biot's seminal paper [11]:

$$F(\lambda) = \frac{(\lambda \sqrt{-i})^2 (1 - H(\lambda))}{3 H(\lambda)} \quad (2)$$

$$H(\lambda) = 1 - \tanh(\lambda \sqrt{-i}) / (\lambda \sqrt{-i}) \quad (3)$$

$$\lambda = \sqrt{\frac{3\rho_f \omega q^2}{\Omega \sigma}} \quad (4)$$

,where angular frequency, tortuosity, porosity and flow resistivity are symbolised by ω , q^2 , Ω and σ respectively. i is the imaginary unit of $\sqrt{-1}$ and the harmonic motion of $\exp(-i\omega t)$ is assumed with time denoted by t . When the wavelength of interest is much larger than the typical sizes of soil particles and pores, the characteristic equations of the wave numbers for type-I (l_1) and -II (l_2) compressional waves and a shear wave (l_3) may be written in the Biot-Stoll formulation [14]:

$$\begin{vmatrix} H l_{1,2}^2 - \rho \omega^2 & \rho_f \omega^2 - C l_{1,2}^2 \\ \rho_f \omega^2 - C l_{1,2}^2 & m_a \omega^2 - M l_{1,2}^2 + i\omega F\sigma \end{vmatrix} = 0, \quad (5)$$

$$\begin{vmatrix} \rho \omega^2 - \mu l_3^2 & \rho_f \omega^2 \\ \rho_f \omega^2 & m_a \omega^2 + i\omega F\sigma \end{vmatrix} = 0. \quad (6)$$

The coefficients H , C , and M are re-formulations of the elastic constants P , Q , and R appearing in Biot's theory, and the detailed formulae can be found in Ref. [14]. m_a is an apparent mass defined by $q^2 \rho_f / \Omega$. And μ is the complex shear modulus, represented by N in Biot's original notation of P , Q , R , and N .

Since the pore-fluid related parameters are well defined for a certain idealised model for pore shape, the remaining parameters in solving the characteristic equations (Eqs. (5) and (6)) are mainly structure-related. They are flow resistivity, complex bulk and shear moduli of the porous structure, and tortuosity.

2.2 Wave-propagation model

Once wave numbers of three types of elastic waves are found, the reflection and refraction of waves on layer interfaces can be determined by solving a boundary value problem. When an airborne acoustic source is placed above infinite plane interface, the resulting wave field can be considered as axisymmetric. The wave motion according to Helmholtz equation may be represented by using displacement potentials (Ψ) [12]:

$$\nabla^2 \Psi_{m,n}(r, z) + l_{m,n}^2 \Psi_{m,n}(r, z) = \delta_n(r, z). \quad (7)$$

The second subscript n denote a layer. The first subscript m indicates the wave types: 0 for a wave in the air layer above the ground; 1 and 2 for two compressional waves, 3 for a shear wave in a soil layer. The wave number of soils (l_m for $m = 1, 2, 3$) are obtained by Eqs. (5) and (6). The wave number for air layer is $l_0 = \omega / c_f$, where c_f is the speed of sound in air. A point source in a layer n is expressed by δ_n . Due to the nature of axisymmetric field, by applying Hankel transform, the vertical dimension (z) can be separated from the radial dimension (r). The forward Hankel transform applied in the radial dimension is:

$$\psi_{m,n}(\xi, z) = \int_0^\infty \Psi_{m,n}(r, z) J_0(l_r r) r dr \quad (8)$$

,where $J_0(\cdot)$ is the zeroth-order Bessel functions of the first kind with a complex argument. ξ is the projection of wave number to the surface and is usually referred to as horizontal wave number. The transformed quantity ($\psi_{m,n}$) in the left-hand side is a Green's function which is dependent on depth but independent of range. Full execution of Hankel transform to Eq. (7) now leads to the following ordinary differential equation which is independent of range and is uniquely determined at a given depth (h):

$$\frac{d^2}{dz^2} \psi_{m,n}(\xi, h) + \beta_{m,n}^2 \psi_{m,n}(\xi, h) = \delta_n(h), \quad (9)$$

$$\beta_{m,n}^2 = l_{m,n}^2 - \xi^2.$$

These Green's functions are built with details such as the location of a source and the amplitudes of propagating waves. For a monopole source near plane interface, the contribution from the source and the interaction with the boundary are essentially the Sommerfeld representation. And Green's functions defined at all the layers need to be calculated together by constructing a global matrix [12]. This is a system of

linear equations composed of boundary conditions of all layers. For an air-soil boundary, four boundary conditions are to be met: continuity of air pressure, normal displacement, normal stress and tangential stress. For a soil-soil boundary, two more boundary conditions are required: continuity of normal relative fluid displacement and tangential frame displacement.

Once the Green's function is found for each layer as a function of depth of interest by Eq. (9), the displacement potentials ($\Psi_{m,n}$) at a range of interest (R) can be obtained through the inverse Hankel transform:

$$\Psi_{m,n}(R, h) = \int_0^\infty \psi_{m,n}(\xi, h) J_0(\xi R) \xi d\xi \quad (10)$$

Finally, the displacement potentials are converted back to particle displacements of corresponding phase, from which acoustic pressure and soil particle velocities are further calculated [12].

2.3 Measurements

For a monopole acoustic source, we have used a compression driver extended by a metal pipe with an internal diameter of 2 cm. For the detection of sound field in air, two precision microphones (Brüel & Kjær model) have been placed above soils and vertically separated. For the monitoring of the soil surface vibration, a laser Doppler vibrometer (Polytec model) has been deployed with the laser beam obliquely incident to the surface.

The generation and acquisition of data have been made using a National Instruments data acquisition (DAQ) board controlled by a Matlab data acquisition toolbox. A generated electrical source signal is enhanced via a power amplifier before reaching the compression driver. Microphone signals are also amplified before an analogue-to-digital converter. The laser signal is conditioned within its controller unit. Then, signals from the microphones and the LDV are digitised in the DAQ board. These time-domain signals are then converted to frequency domain through discrete Fourier transform. Finally, three transfer functions are evaluated: two A-S coupling for the ratio of the LDV output to each microphone signal and a level difference between two microphone readings. These transfer functions are later used for deducing the soil parameters.

2.4 Optimisation

During measurements, we have arranged two microphones and an LDV, and hence three transfer functions between them are evaluated for each measurement dataset. An optimisation algorithm has been run to find a parameter combination to minimise the differences of all three pairs of the measured and the simulated transfer functions (TF):

$$\sum_{p=1}^{p=3} \sum_f (|TF_{mea,p}(f)| - |TF_{sim,p}(f)|)^2. \quad (11)$$

The subscripts mea and sim denote the measured and the simulated transfer functions. The simulation is carried out using the wave propagation model introduced earlier. The variable f is the temporal frequency, and the type of a transfer function is indicated by a subscript p . The difference is calculated based on the magnitudes of complex transfer functions. We

have found that the optimisation is more effective if only the magnitudes of the transfer functions are used rather than the full complex domain data. This may be because enveloping the complex data effectively smooths the measured data.

For optimisation problems, it is useful if a search space can be visualised in simulation. For a multi-dimensional optimisation, however, it is not straightforward to plot the search space of all variables in a single intuitive image. Instead, one variable (i.e., one-dimensional) or a pair of variables (i.e., two-dimensional) can be chosen at a time while the rest of variables are fixed.

Figure 1 shows the simulation of a cost function with uniformly varying porosity while the rest of parameters are fixed. The simulated data for the cost function is the A-S coupling transfer function between signals from imaginary microphone and LDV. The overall shape of the cost function can be considered to be convex and well-posed. The cost function for the real part of bulk modulus of soil structure is shown in Figure 2. The search space is not as smooth as that of the porosity.

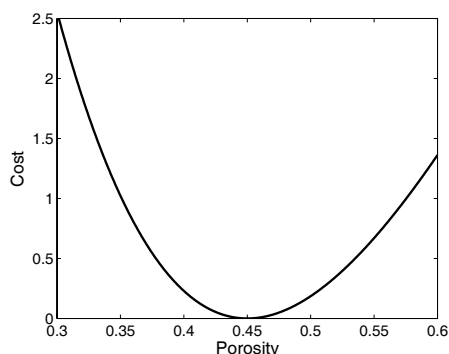


Figure 1: Simulation of a cost function of acoustic-to-seismic coupling transfer function for the porosity while other parameters are fixed. The exact value of the porosity is 0.45.

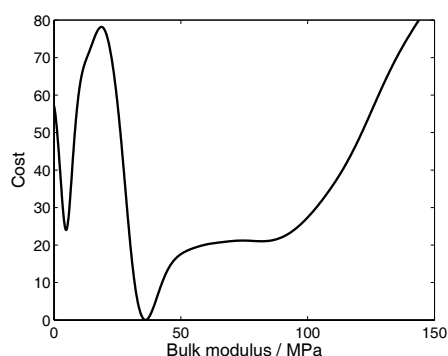


Figure 2: Simulation of a cost function of acoustic-to-seismic coupling transfer function for the real part of bulk modulus while other parameters are fixed. The exact value of the modulus is 36 MPa.

When the outcomes in Figures 1 and 2 are treated as one-dimensional optimisation problems on their own, cost functions in the kind of Figure 1 can be easily addressed with a local-search algorithm, while one may need a global-search algorithm for the kind in Figure 2. When the optimisation problem is multi-dimensional, it is anticipated the complexity of the total search space can be increased immensely.

As a result of the tortuous structure of the overall search space, it has been found that a single or a few executions of optimisation algorithms, regardless of local or global methods, are not up for the task addressed in this paper. An effective strategy we have found is simply to run local-search algorithms as many times as possible with different initial guesses to start the algorithm.

For the current work, we have created a Latin hypercube [15] to uniformly spread the initial guesses. For each initial seed, we have run the Rosenbrock algorithm [16] for a local search. We have then chosen the first few best solutions obtained by all sets of local searches for further examination. Since the initial guesses are uniformly spaced by the Latin hypercube sampling, most of the search space can be assessed equally and more efficiently than by random guesses, and the chance of reaching the global solution can be increased.

3 Results

The measurements have been conducted both indoors and outdoors. The indoor measurements were carried out in a semi-anechoic chamber. The outdoor measurements were conducted at a field. Both places are located at the Open University, United Kingdom.

For indoor applications, we have carried out measurements over dry sand filled in an aluminium tray ($1 \text{ m} \times 1 \text{ m} \times 0.11 \text{ m}$) placed on a concrete floor in a semi-anechoic chamber. The particle size of the sand was graded between 0.5 and 1.0 mm. The rest of the floor was covered with plastic foam wedges to reduce the unwanted reflection of sounds.

Outdoors, we constructed a trench with the size of $2 \text{ m} \times 2 \text{ m} \times 0.47 \text{ m}$ within the premises of the Open University. Concrete substrate with a few centimetre in thickness was laid on the bottom to define an acoustically impervious rigid boundary. No treatment was made for the four sides. The trench was filled with builder's sand whose particle size was not graded. The area is surrounded by mainly clay soils covered with grass.

Figure 3 compares the A-S transfer functions for the measurement and the simulation for dry sand sample at a semi-anechoic chamber. The heights of the source and the microphone were 9 and 14 cm. The distances from the source to the LDV focus and to the microphone were 18 and 43 cm. The incident angle of the laser beam was 51° . The deduced parameter values are shown in Table 1.

Figure 4 compares the A-S transfer functions for the measurement and the simulation for sand at an outdoor trench. The heights of the source and the microphone were 23 and 29 cm. The distances from the source to the LDV focus and to the microphone were 51 and 106 cm. The incident angle of the laser beam was 58° . For Figure 4, the sand sample was assumed to be a single homogenous layer above the concrete substrate. The deduced parameter values are shown in Table 1.

Figure 5 shows the improved fitting when the sand sample inside the trench was assumed to consist of two layers. The depth of the top layer was also deduced while the total depth of the two layers was kept as 47 cm. The deduced parameter values are shown in Table 1.

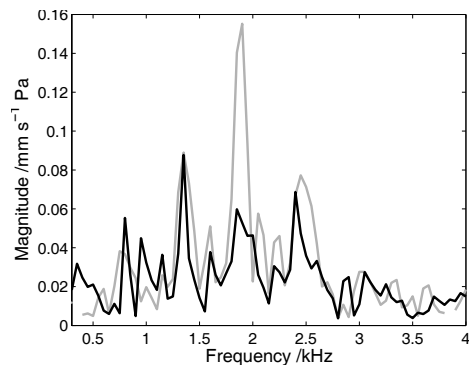


Figure 3: Comparisons of the measured (in grey) and the simulated acoustic-to-seismic coupling (in black) based on the deduced parameters for dry sand at a laboratory. Part of the measured data is missing due to poor signal return for the LDV.

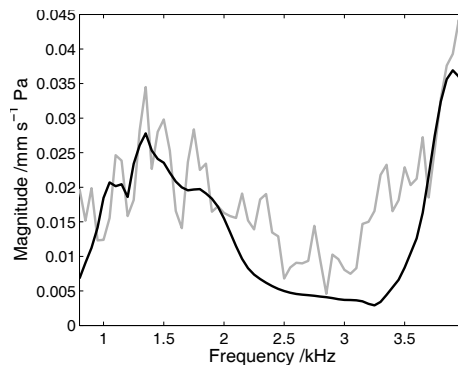


Figure 5: Comparisons of the measured (in grey) and the simulated acoustic-to-seismic coupling (in black) based on the deduced parameters for outdoor sand trench. Two layers were assumed for the simulation.

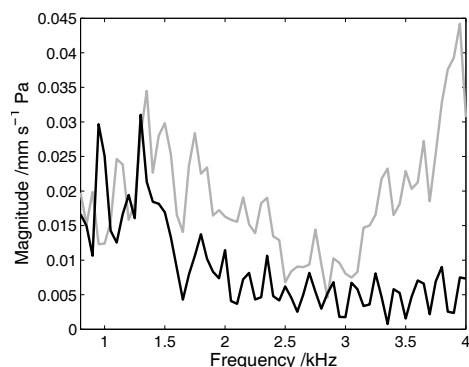


Figure 4: Comparisons of the measured (in grey) and the simulated acoustic-to-seismic coupling (in black) based on the deduced parameters for outdoor sand trench. A single layer was assumed for the simulation.

4 Conclusion

The feasibility of using measurements of acoustic-to-seismic (A-S) coupling to deduce the physical parameters of soils has been investigated both in the laboratory and outdoors in a trench. The determined soil parameters were flow resistivity, porosity, complex bulk and shear moduli of soil structure. For soils which were better described by two layers than one, the depth of the top layer was also estimated. A compression driver extended with a tube was used to emulate a monopole acoustic source. The resulting sound field was recorded by two precision microphones and the induced soil particle velocity was measured by a laser Doppler vibrometer. Three pairs of the measured transfer functions were compared to the simulated counterparts evaluated by a numerical model incorporating Biot poroelasticity theory and wave propagation model in layered media. An optimisation algorithm was used to find a set of soil parameters which minimise the difference between the measured and the simulated transfer functions. Latin hypercube was adopted for uniform sampling of initial guesses. It was shown that dual-layer analysis produced better agreement than single-layer assumption for outdoor soils. The current work has demonstrated that soils can be characterised non-invasively through A-S coupling.

Table 1: Parameter values used to plot the simulated acoustic-to-seismic coupling transfer functions in Figures 3, 4 and 5. Assumed values are annotated with †, and the rest are deduced through optimisation.

	Dry sand	Single-layer trench	Dual-layer trench	
			Layer 1	Layer 2
Flow resistivity /kPa s m ⁻²	141.6	152.8	139.6	1686.6
Porosity	0.42	0.34	0.34	0.26
Bulk modulus /MPa	16.0	24.2	29.8	432.1
Shear modulus /MPa	3.2	15.4	11.5	50.2
Loss factor	0.010	0.001	0.004	0.059
Depth /cm	11.0 [†]	47.0 [†]	3.5	43.5 [†]

Acknowledgments

This work was funded by the UK Engineering and Physical Sciences Research Council (grant EP/H040617/1).

References

- [1] W. P. Arnott, J. M. Sabatier. “Laser-doppler vibrometer measurements of acoustic to seismic coupling”. *Applied Acoustics* **30**(4), 279–291 (1990)
- [2] N. Xiang, J. M. Sabatier. “An experimental study on antipersonnel landmine detection using acoustic-to-seismic coupling”. *Journal of the Acoustical Society of America* **113**(3), 1333–1341 (2003)
- [3] K. Attenborough. “Review of ground effects on outdoor sound propagation from continuous broadband sources”. *Applied Acoustics* **24**(4), 289–319 (1988)

- [4] K. Attenborough, K. M. Li, K. Horoshenkov. *Predicting Outdoor Sound*. Taylor & Francis, London (2007)
- [5] S. Taherzadeh, K. Attenborough. “Deduction of ground impedance from measurements of excess attenuation spectra”. *Journal of the Acoustical Society of America* **105**(3), 2039–2042 (1999)
- [6] H. M. Hess, K. Attenborough, N. W. Heap. “Ground characterization by short-range propagation measurements”. *Journal of the Acoustical Society of America* **87**(5), 1975–1986 (1990)
- [7] L. M. Brekhovskikh. *Waves in Layered Media*. Academic Press, New York (1960)
- [8] C. F. Chien, W. W. Soroka. “Sound propagation along an impedance plane”. *Journal of Sound and Vibration* **43**, 9–20 (1975)
- [9] K. M. Li, T. Waters-Fuller, K. Attenborough. “Sound propagation from a point source over extended-reaction ground”. *Journal of the Acoustical Society of America* **104**(2), 679–685 (1998)
- [10] J. M. Sabatier, H. E. Bass, L. N. Bolen, K. Attenborough, V. V. S. S. Sastry. “The interaction of airborne sound with the porous ground: The theoretical formulation”. *Journal of the Acoustical Society of America* **79**(5), 1345–1352 (1986)
- [11] M. A. Biot. “Theory of propagation of elastic waves in a fluid-saturated porous solid. I. low-frequency range, II. higher frequency range”. *Journal of the Acoustical Society of America* **28**(2), 168–191 (1956)
- [12] S. Tooms, S. Taherzadeh, K. Attenborough. “Sound propagation in a refracting fluid above a layered fluid-saturated porous elastic material”. *Journal of the Acoustical Society of America* **93**(1), 173–181 (1993)
- [13] N. Harrop, K. Attenborough. “Laser-doppler vibrometer measurements of acoustic-to-seismic coupling in unconsolidated soils”. *Applied Acoustics* **63**(4), 419–429 (2002)
- [14] R. D. Stoll. “Acoustic waves in saturated sediments”. In: L. Hampton, ed., “Physics of Sound in Marine Sediments”, 19–39. Plenum Press, New York (1974)
- [15] A. I. J. Forrester, A. Sóbester, A. J. Keane. *Engineering Design via Surrogate Modelling: A Practical Guide*. John Wiley & Sons, Chichester (2008)
- [16] H. H. Rosenbrock. “An automatic method for finding the greatest or least value of a function”. *Computer Journal* **3**(3), 175–184 (1960)